Composite Structures 142 (2016) 200–214

Contents lists available at ScienceDirect

Composite Structures

journal homepage: www.elsevier.com/locate/compstruct

Transient analysis of stationary interface cracks in orthotropic bi-materials using oscillatory crack tip enrichments

Arman Afshar, Saeed Hatefi Ardakani, Soheil Mohammadi *

High Performance Computing Laboratory, School of Civil Engineering, University of Tehran, Tehran, Iran

ARTICLE INFO

Article history:
Available online 25 January 2016

Keywords:
Dynamic loading
Partition of unity enrichments
Mixed-mode interface fracture
Orthotropic bi-materials
Oscillatory stress and displacement fields
Interaction integral method

ABSTRACT

The problem of an interface crack between two orthotropic layers under dynamic loading is analyzed. Special crack tip enrichment functions are incorporated into the standard finite element shape functions to exactly reproduce oscillatory stress and displacement fields near the tip of the interface crack. Moreover, kinematics of displacement and its gradients across the crack face and material interface are also modeled by partition of unity enrichments. Special attention is given to extraction of stress intensity factors by utilizing a proper form of the interaction integral for orthotropic bi-materials. Advantages of this method of extracting stress intensity factors over the conventional displacement extrapolation technique are discussed. Several bi-material configurations with both vanishing and non-vanishing oscillatory indexes are solved using the interaction integral and the results are compared with the available data in the literature. Effects of employing oscillatory crack tip enrichments and validation of the path-independent J-integral are also discussed.

1. Introduction

Combination of individual constituents to utilize the advantages of each material has made composite materials ubiquitous in different branches of engineering, from aerospace and automotive structures to electronic packages. Nonetheless, the inherent weakness associated with the interface joining each material might limit the use of composites, particularly in extreme loading conditions. In the engineering community, interface cracks have been considered as one of the main sources of failure in composite materials, making an accurate analysis of these particular defects necessary. As many applications of composite materials include time-dependent and impact loadings, the current study is focused on analysis of interface cracks under dynamic loadings.

In case of fiber reinforced composite materials, the interface crack is located between layers that are not isotropic, causing a complex stress and displacement field near the tip of an interface crack. Since arbitrary loadings and geometries encountered in a practical engineering problem inhibit the use of analytical methods, numerical techniques must be employed to tackle these problems. A numerical technique widely used in the literature to analyze problems with singularity and discontinuities is the boundary element method (BEM), which makes use of fundamental solutions to accurately simulate complex problems. However, since the fundamental solution for general layered anisotropic media does not exists, Refs. [1–5] utilized the solution of homogeneous anisotropic media in a multi-domain BEM framework to analyze interface cracks under static loading condition. In addition to BEM mentioned above, another numerical technique for numerical analysis of fracture problems is the meshfree method (Refs. [6,7]).

For the cases of dynamic loading, the situation becomes more complicated and only a limited number of investigations can be found [8,9], which suffer from poor stability in the time domain, as mentioned in Ref. [10]. A more stable algorithm was presented by Lei et al. [10], but this work neglected the oscillatory crack tip fields near interface cracks. Song et al. [11] made an improvement and utilized the scaled boundary finite element method to reproduce the mentioned oscillatory fields. It should be also noted that nearly all mentioned BEM-based works utilize the conventional displacement extrapolation technique to extract stress intensity factors, which further requires accurate simulation of crack tip fields. In the case of interface cracks, however, obtaining accurate crack tip displacements is cumbersome, if not impossible. Also, Domain discretization in scaled boundary elements also requires especial care (Refs. [12,13]).

Finite element method (FEM), on the other hand, can readily deal with arbitrary geometries, and many unconditionally stable time integration algorithms do exist for analysis of dynamic problems.

* Corresponding author. Tel.: +98 21 6111 2258; fax: +98 21 6640 3808.
E-mail address: smoham@ut.ac.ir (S. Mohammadi).

http://dx.doi.org/10.1016/j.compstruct.2016.01.086
0263-8223/

It is also well suited for post-processing evaluation of J-integral, by which the stress intensity factors can be easily obtained. Nevertheless, while the standard finite element method proved to be successful in common fracture mechanics simulations, the fundamental complications associated with oscillatory stress and displacement fields near the tip of an interface crack, especially in the case of layered orthotropic media, result in its low performance and accuracy. Recently, an algorithm called "the edge rotation algorithm" was proposed for fracture analysis based on FEM. In this simple algorithm, an alternative method to the methods based on enrichment techniques was proposed (Refs. [14,15]).

A remedy is the extended finite element method (XFEM) [16,17], by which the exact crack tip fields can be precisely simulated. Preserving all advantages of FEM over BEM, the XFEM formulation presented here reproduces the exact oscillatory crack tip fields. It also represents the kinematics of strong and weak discontinuity easily. XFEM has been successfully used for static and dynamic fracture analysis of homogeneous orthotropic materials [18–25], and static fracture analysis of isotropic and orthotropic bi-materials [26–28]. As many applications of composite materials include time-dependent and impact loadings, the current study is focused on analysis of interface cracks under dynamic loadings. Therefore, an existing XFEM methodology [27] is further extended to dynamic analysis of interface cracks in orthotropic bi-materials, with particular attention to the effects of oscillatory fields and the interaction integral. Also, it should be noted that prior to the present methods, FEM and BEM solutions developed for analysis of interface cracks under dynamic loadings without the need for any exact solution for distribution of stress and displacement fields around a crack tip. In the current study, however, the exact analytical distribution of displacement and stress fields are introduced for the first time in the dynamic analysis of interface crack and the differences between the proposed method and other numerical methods are demonstrated.

The organization of this work is as follows: First, a description of basics of the considered problem and essential backgrounds of interface fracture mechanics under the assumption of linear elastic fracture mechanic (LEFM) are provided. The next section explains how strong and weak discontinuities and oscillatory crack tip fields are modeled in the context of XFEM. Then, a brief review of the discretized equations and numerical evaluation of crack tip parameters are presented, followed by several numerical simulations to study the effects of employed crack tip enrichments and the interaction integral method. The paper is closed with the concluding remarks.

2. Problem statement

As illustrated in Fig. 1, the elastodynamic problem of a layered orthotropic body containing an interface crack is considered in this study:

$$\mathrm{Div}(\boldsymbol{\sigma}) + \mathbf{f} = \rho\ddot{\mathbf{u}} \tag{1}$$

with the following boundary conditions

$$\mathbf{u}(\mathbf{x}, t) = \bar{\mathbf{u}}(\mathbf{x}, t) \quad \text{on } \Gamma_u \tag{2}$$

$$\boldsymbol{\sigma}\cdot\mathbf{n} = \bar{\mathbf{t}} \quad \text{on } \Gamma_t \tag{3}$$

and the initial conditions

$$\mathbf{u}(\mathbf{x}, 0) = \mathbf{u}_0 \tag{4}$$

$$\dot{\mathbf{u}}(\mathbf{x}, 0) = \dot{\mathbf{u}}_0 \tag{5}$$

The Hook's law in plane stress conditions for both linear elastic orthotropic materials are [29]

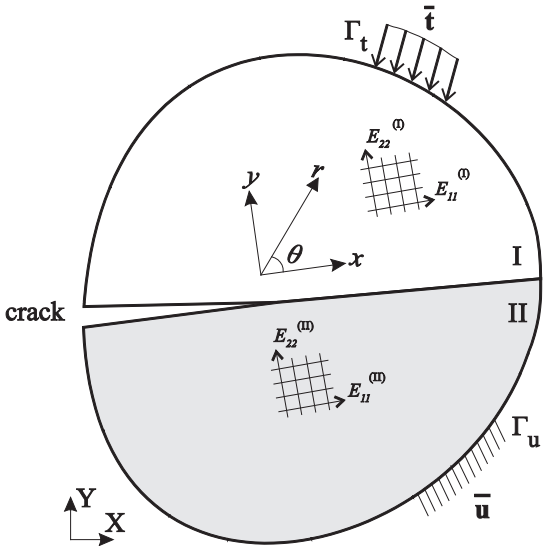

Fig. 1. An interface crack in a layered orthotropic material subjected to dynamic loading.

$$\begin{Bmatrix}\varepsilon_{11}\\ \varepsilon_{22}\\ 2\varepsilon_{12}\end{Bmatrix} = \begin{bmatrix}a_{11} & a_{12} & a_{16}\\ a_{21} & a_{22} & a_{26}\\ a_{61} & a_{62} & a_{66}\end{bmatrix}\begin{Bmatrix}\sigma_{11}\\ \sigma_{26}\\ \sigma_{12}\end{Bmatrix} = \begin{bmatrix}D_{1111} & D_{1122} & 2D_{1112}\\ D_{2211} & D_{2222} & 2D_{2212}\\ 2D_{1211} & 2D_{1222} & 4D_{1212}\end{bmatrix}\begin{Bmatrix}\sigma_{11}\\ \sigma_{26}\\ \sigma_{12}\end{Bmatrix} \tag{6}$$

In plane strain conditions, the following replacement should be done:

$$a_{ij} \to a_{ij} - \frac{a_{i3}-a_{3i}}{a_{33}} \quad i,j = 1,2,6 \tag{7}$$

The differential equation including equilibrium, orthotropic constitutive law, and compatibility equation has a characteristic equation of the form [30]

$$t^4 + 2B_{12}t^2 + K_{66} = 0 \tag{8}$$

with

$$B_{12} = \frac{2a_{12}+a_{66}}{2a_{11}} \text{ and } K_{66} = \frac{a_{22}}{a_{11}} \tag{9}$$

Most of the orthotropic materials, including all simulated problems, have properties that ensure $\sqrt{K_{66}} < B_{12}$, resulting in purely imaginary roots of Eq. (8), in the form of

$$t_1 = ip;\ t_2 = iq \quad \text{if } \sqrt{K_{66}} < B_{12} \tag{10}$$

with

$$p = \sqrt{B_{12} - \sqrt{B_{12}^2 - K_{66}}};\quad q = \sqrt{B_{12} + \sqrt{B_{12}^2 - K_{66}}} \tag{11}$$

For further information and discussion on various types of composites, see Ref. [27].

3. Interface crack mechanics

Consider an interface crack located between two orthotropic layers. The definition of stress intensity factors for interface cracks, proposed by Cho et al. [2], is adopted. Based on this definition, the singular stress at a distance r ahead of the crack tip can be written as

$$[\,\tau_{xy} \quad \sigma_{yy}\,]_{r,\theta=0} = \frac{1}{\sqrt{2\pi r}}\mathrm{Re}\left[\mathbf{K}\mathbf{W}\left(\frac{r}{L}\right)^{i\varepsilon}\right] \tag{12}$$

where $\mathbf{K} = K_1 + iK_2$ is the complex stress intensity factor, $\mathbf{W}$ is a material property vector defined later, L is the characteristic length of the interface crack, and ε is the oscillatory index. It should be noted that due to the coupling of shear and tensile behaviors near the tip of interface cracks with $\varepsilon \neq 0$, K_1 and K_2 cannot be rigorously interpreted as the conventional mode-I and mode-II stress intensity factors [31]. The choice of characteristic length is somehow arbitrary, and the half crack length, adopted by [11], is chosen in this work. The oscillatory index ε is defined as

$$\varepsilon = \frac{1}{2\pi} \ln\left(\frac{1-\beta}{1-\beta}\right) \tag{13}$$

where β is the Dundur's parameter [32]:

$$\beta = \frac{-\mathrm{H}_{12}}{\sqrt{\mathrm{H}_{11}\mathrm{H}_{22}}} \tag{14}$$

where H_{ij} are the components of the Hermitian matrix $\mathbf{H}$ for bi-materials:

$$\mathbf{H} = \begin{bmatrix} \frac{k_{22}^{\mathrm{I}}\sqrt{2(1+s_1)/\varphi_1}}{\mathbf{C}_{66}^{\mathrm{I}}R_1} + \frac{k_{22}^{\mathrm{II}}\sqrt{2(1+s_2)/\varphi_2}}{\mathbf{C}_{66}^{\mathrm{II}}R_2} & i\left(\frac{k_{22}^{\mathrm{I}}-k_{12}^{\mathrm{I}}/\varphi_1}{\mathbf{C}_{66}^{\mathrm{I}}R_1} - \frac{k_{22}^{\mathrm{II}}-k_{12}^{\mathrm{II}}/\varphi_2}{\mathbf{C}_{66}^{\mathrm{II}}R_2}\right) \\ -i\left(\frac{k_{22}^{\mathrm{I}}-k_{12}^{\mathrm{I}}/\varphi_1}{\mathbf{C}_{66}^{\mathrm{I}}R_1} - \frac{k_{22}^{\mathrm{II}}-k_{12}^{\mathrm{II}}/\varphi_2}{\mathbf{C}_{66}^{\mathrm{II}}R_2}\right) & \frac{k_{22}^{\mathrm{I}}\sqrt{2(1+s_1)\varphi_1}}{\mathbf{C}_{66}^{\mathrm{I}}R_1} + \frac{k_{22}^{\mathrm{II}}\sqrt{2(1+s_2)\varphi_2}}{\mathbf{C}_{66}^{\mathrm{II}}R_2} \end{bmatrix} \tag{15}$$

with

$$k_{ij}^{\alpha} = \frac{\mathbf{C}_{ij}^{\alpha}}{\mathbf{C}_{66}^{\alpha}}; \quad \varphi_{\alpha} = \sqrt{\frac{k_{11}^{\alpha}}{k_{22}^{\alpha}}}; \quad \alpha = \begin{cases} I & \text{(lower material)} \\ \mathrm{II} & \text{(upper material)} \end{cases} \tag{16}$$

$$s_{\alpha} = \frac{1 + k_{11}^{\alpha}k_{22}^{\alpha} - \left(1 + k_{12}^{\alpha}\right)^2}{2\sqrt{k_{11}^{\alpha}k_{22}^{\alpha}}} \tag{17}$$

$$R_{\alpha} = \left(k_{22}^{\alpha}\right)^2\varphi_{\alpha} - \frac{\left(k_{12}^{\alpha}\right)^2}{\varphi_{\alpha}} \tag{18}$$

where $\mathbf{C}_{ij}^{\alpha}$ are the elements of the elasticity matrix of material α (inverse of the compliance matrix in Eq. (6)), and $\mathbf{W}$ in Eq. (12) is a complex vector for orthotropic bi-materials [11]:

$$\mathbf{W} = \begin{bmatrix} -\mathrm{i} & \frac{\sqrt{H_{11}H_{22} - H_{12}^2}}{H_{22}} \end{bmatrix} \tag{19}$$

Finally, the energy release rate and phase angle can be related to $\mathbf{K}$ using the following equations [32]

$$G = \frac{H_{22}|\mathbf{K}|^2}{4\cosh^2(\pi\varepsilon)} \tag{20}$$

$$\psi = \mathrm{Arctan}\left(\frac{\tau_{xy}}{\eta\sigma_{yy}}\right)_{r=L} = \mathrm{Arctan}\left(\frac{\mathrm{Im}[\mathbf{K}L^{i\varepsilon}]}{\mathrm{Re}[\mathbf{K}L^{i\varepsilon}]}\right) \tag{21}$$

where $\eta = \sqrt{H_{22}/H_{11}}$ is the traction resolution factor.

4. Displacement approximation in XFEM formulation

In XFEM, the displacement field is enriched by special functions in order to accurately reproduce the analytical asymptotic fields near the crack tips, and to provide the appropriate discontinuity in the domain of finite element approximation. In the case of interface cracks, the displacement field is approximated by

$$\begin{aligned} \mathbf{u}(\mathbf{x}) &= \sum_{n\in N}\varphi_n^{\mathrm{d}}\mathbf{d}_n + \sum_{i\in M_{\mathrm{crack}}}\varphi_i^{\mathrm{a}}\mathbf{a}_i + \sum_{j\in M_{\mathrm{tip}}}\varphi_j^{\mathrm{b}}\mathbf{b}_j + \sum_{k\in M_{\mathrm{interface}}}\varphi_k^{c}\mathbf{c}_k \\ &= \sum_{n\in N}N_n(\mathbf{x})\mathbf{d}_n + \sum_{i\in M_{\mathrm{crack}}}N_i(\mathbf{x})H(\mathbf{x})\mathbf{a}_i \\ &\quad + \sum_{j\in M_{\mathrm{tip}}}N_j(\mathbf{x})\left(\sum_t \mathbf{b}_j F_t(\mathbf{x})\right) + \sum_{k\in M_{\mathrm{interface}}}N_k(\mathbf{x})\chi_k(\mathbf{x})\mathbf{c}_k \end{aligned} \tag{22}$$

where N, M_{crack}, M_{tip}, and $M_{\mathrm{interface}}$ denote the set of conventional, crack face, crack tip, and interface nodes, respectively (Fig. 2). $\varphi_n^{\mathrm{d}}, \varphi_i^{\mathrm{a}}, \varphi_j^{\mathrm{b}}, \varphi_k^{c}$ are also standard, strong discontinuity, crack tip singularity, and weak discontinuity shape functions. Accordingly, $\mathbf{a}_i$, $\mathbf{b}_j$, and $\mathbf{c}_k$ are the vectors of additional degrees of freedom for crack face, crack tip, and interface nodes. $H(\mathbf{x})$ is the Heaviside function, used for modeling crack face strong discontinuity (illustrated in Fig. 3):

$$H(x) = \begin{cases} +1 & \text{points above the crack} \\ -1 & \text{points below the crack} \end{cases} \tag{23}$$

$F_t(\mathbf{x})(t = 1-8)$ are the eight tip enrichment functions, derived from the asymptotic fields of an interface crack between two orthotropic materials, incorporated into the finite element displacement field in order to exactly reproduce the complex oscillatory behavior around the crack tip [27]:

$$F(r,\theta) = \begin{Bmatrix} e^{-\varepsilon\theta_l}\cos(\varepsilon ln(r_l) + \frac{\theta_l}{2})\sqrt{r_l} & e^{-\varepsilon\theta_l}\sin(\varepsilon ln(r_l) + \frac{\theta_l}{2})\sqrt{r_l} \\ e^{\varepsilon\theta_l}\cos(\varepsilon ln(r_l) - \frac{\theta_l}{2})\sqrt{r_l} & e^{\varepsilon\theta_l}\cos(\varepsilon ln(r_l) - \frac{\theta_l}{2})\sqrt{r_l} \\ e^{-\varepsilon\theta_s}\cos(\varepsilon ln(r_s) + \frac{\theta_s}{2})\sqrt{r_s} & e^{-\varepsilon\theta_s}\sin(\varepsilon ln(r_s) + \frac{\theta_s}{2})\sqrt{r_s} \\ e^{\varepsilon\theta_s}\cos(\varepsilon ln(r_s) - \frac{\theta_s}{2})\sqrt{r_s} & e^{\varepsilon\theta_s}\cos(\varepsilon ln(r_s) - \frac{\theta_s}{2})\sqrt{r_s} \end{Bmatrix} \tag{24}$$

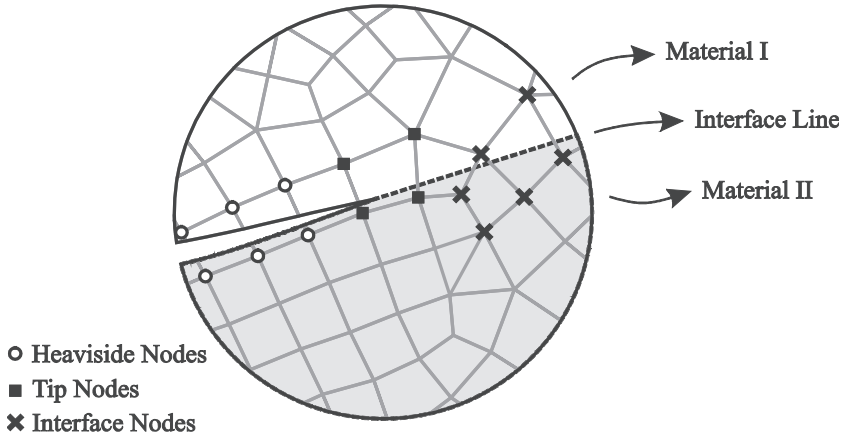

Fig. 2. Adopted strategy for selecting enriched nodes of an interface crack.

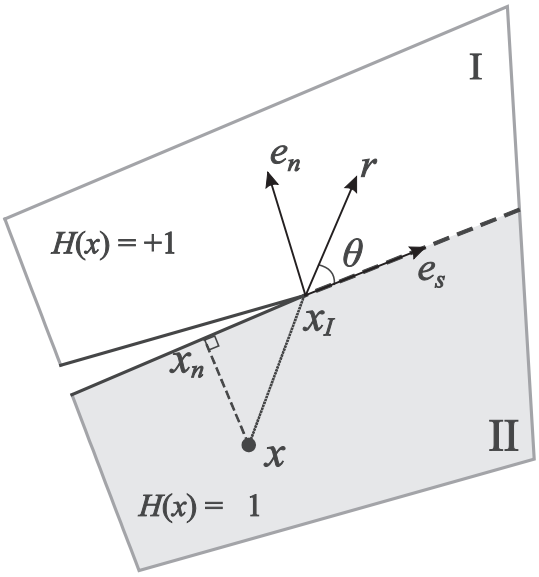

Fig. 3. Definition of the signed distance functions for strong and weak discontinuity enrichments.

$$r_j = r\sqrt{\cos^2\theta + z_j^2 \sin^2\theta}; \quad \theta_j = \arctan(z_j\, tan\,\theta)$$
$$j = l, s; \quad z_l = p,\ z_s = q \tag{25}$$

where p and q are defined in Eq. (11). r and θ are polar coordinates measured from the crack tip, as illustrated in Fig. 1.

Returning to Eq. (22), χ_k is the weak discontinuity enrichment function, used to provide the discontinuity in the strain field in a non-conformal mesh, i.e. the mesh in which the element edges are not conformed to the material interface:

$$\chi_k = \min \|\mathbf{x} - \mathbf{x}_n\| \cdot \text{sign}(\mathbf{e}_n.(\mathbf{x} - \mathbf{x}_n)) \tag{26}$$

where $\mathbf{x}, \mathbf{x}_\eta,$ and $\mathbf{e}_n$ are defined in Fig. 3. More details about weak discontinuity are available in Ref. [33].

5. Discretized equilibrium equation and time integration

The discretized weak form of the dynamic equilibrium equation (Eq. (1)) at time n is

$$\mathbf{M}\ddot{\mathbf{u}}_n + \mathbf{C}^{\mathrm{d}}\dot{\mathbf{u}}_n + \mathbf{K}\mathbf{u}_n = \mathbf{f}_n \tag{27}$$

where $\mathbf{M}, \mathbf{C}^{\mathrm{d}},$ and $\mathbf{K}$ are the mass, damping, and stiffness matrices, respectively, and $\mathbf{f}$ is the force vector. $\ddot{\mathbf{u}}, \dot{\mathbf{u}},$ and $\mathbf{u}$ are the XFEM acceleration, velocity and displacement vectors, respectively:

$$\mathbf{u} = \{\mathbf{d} \quad \mathbf{a} \quad \mathbf{b} \quad \mathbf{c}\}^{\mathrm{T}} \tag{28}$$

where $\mathbf{d}$ is the standard vector of nodal displacements, and $\mathbf{a}$, $\mathbf{b}$, and $\mathbf{c}$ are vectors of additional displacements corresponding to oscillatory crack tip enrichments, crack face strong discontinuity and material interface, respectively. The elements of $\mathbf{K}$ and $\mathbf{M}$ matrices and $\mathbf{f}$ vector are

$$\mathbf{K}_{ij}^{rs} = \int_{\Omega^e} (\mathbf{B}_i^r)^{\mathrm{T}} \mathbf{C} (\mathbf{B}_j^s) d\Omega \quad (r, s = d, a, b, c) \tag{29}$$

$$\mathbf{M}_{ij}^{rs} = \int_{\Omega^e} \rho(\varphi_i^r)(\varphi_j^s) d\Omega \quad (r, s = d, a, b, c) \tag{30}$$

$$\mathbf{f}_i^r = \int_{\partial\Omega\cap\partial\Omega} (\varphi_i^r) \bar{\mathbf{t}} d\Gamma \quad (r = d, a, b, c) \tag{31}$$

where $\bar{\mathbf{t}}$ is the applied traction and φ^r represents the XFEM shape functions (see Eq. (22)). $\mathbf{B}$ is the matrix of shape functions derivatives:

$$\mathbf{B}_i^r = \begin{bmatrix} \frac{\partial \varphi^r}{\partial x_i} & 0 \\ 0 & \frac{\partial \varphi^r}{\partial y_i} \\ \frac{\partial \varphi^r}{\partial y_i} & \frac{\partial \varphi^r}{\partial x_i} \end{bmatrix} \quad (r, s = d, a, b, c) \tag{32}$$

Detailed evaluations of these terms within the context of XFEM are available in Ref. [22–24,34]. As depicted in Fig. 4. For the integration of Eq. (29), the sub-domain technique [27] is utilized to partition the three types of enriched elements into sub-triangles. For each sub-triangle in the split and interface elements, 3 Gauss points are utilized. For sub-triangle in the tip element, 7 Gauss points are used.

The classical Rayleigh damping is assumed here

$$\mathbf{C}^{\mathrm{d}} = \gamma_{\mathrm{k}}\mathbf{K} + \gamma_{\mathrm{m}}\mathbf{M} \tag{33}$$

and the unconditionally stable Newmark scheme [35] is utilized for the time integration of Eq. (27).

6. Evaluation of stress intensity factors

The interaction integral method is utilized in this study to evaluate stress intensity factors, based on the auxiliary stress and displacement fields of an interface crack between two orthotropic solids. Since a region far from the crack tip can be selected as the domain of the integral, solutions based on domain integrals are known to be very accurate. Beginning with the definition of the dynamic J-integral [32]

$$J = \int_\Gamma [(W + T)n_1 - \left(\boldsymbol{\sigma} \cdot \frac{\partial \mathbf{u}}{\partial x_1}\right) \cdot \mathbf{n}] \mathrm{d}\Gamma \tag{34}$$

where Γ and $\mathbf{n}$ are the contour enclosing the crack tip and the unit normal of integration path, respectively. W and T are the strain and kinetic energies of the domain within the integration path. For the finite element implementation, Eq. (34) is transformed into

$$J = \int_A \left[\left(\boldsymbol{\sigma} \cdot \frac{\partial \mathbf{u}}{\partial x_1}\right) \frac{\partial q}{\partial \mathbf{x}} - (W + T)\frac{\partial q}{\partial x_1} + \rho \left(\frac{\partial^2 \mathbf{u}}{\partial t^2} \frac{\partial \mathbf{u}}{\partial x_1} - \frac{\partial \mathbf{u}}{\partial t} \frac{\partial^2 \mathbf{u}}{\partial x_1 \partial t} \right) q \right] \mathrm{dA} \tag{35}$$

where A is the area inside Γ. q is an arbitrary function chosen to be unity at the crack tip and zero on Γ. The adopted choice of q-function is of the typical form depicted in Fig. 5. Having defined the J-integral, the interaction integral I can be derived from Eq. (35) in the following manner [32]

$$I = \int_\Gamma \left[\left(\boldsymbol{\sigma} : \boldsymbol{\varepsilon}^{\mathrm{aux}} + \rho \frac{\partial \mathbf{u}}{\partial t} \frac{\partial \mathbf{u}^{\mathrm{aux}}}{\partial t} \right) n_1 - \left(\boldsymbol{\sigma} \cdot \frac{\partial \mathbf{u}^{aux}}{\partial x_1} + \boldsymbol{\sigma}^{\mathrm{aux}} \cdot \frac{\partial \mathbf{u}}{\partial x_1} \right) \cdot \mathbf{n} \right] \mathrm{d}\Gamma \tag{36}$$

For auxiliary terms, the stress and displacement fields of an interface crack are adopted from Ref. [36]. These fields are reported in the appendix of the Esna Ashari and Mohammadi [27]. Numerical evaluation of Eq. (36) for a stationary crack can also be carried out with the help of q-function

$$I = \int_A \left[\left(\boldsymbol{\sigma} \cdot \frac{\partial \mathbf{u}^{\mathrm{aux}}}{\partial x_1} + \boldsymbol{\sigma}^{\mathrm{aux}} \cdot \frac{\partial \mathbf{u}}{\partial x_1} \right) \frac{\partial q}{\partial \mathbf{x}} - \boldsymbol{\sigma} : \boldsymbol{\varepsilon}^{\mathrm{aux}} \frac{\partial q}{\partial x_1} + \rho \frac{\partial^2 \mathbf{u}}{\partial t^2} \cdot \frac{\partial \mathbf{u}^{\mathrm{aux}}}{\partial x_1} q \right] \mathrm{dA} \tag{37}$$

The finite element mesh is adopted to evaluate Eq. (37) using 4×4 gauss quadrature for ordinary elements and the sub-domain technique [27] for enriched ones (Fig. 4). Mixed mode stress intensity factors can then be calculated from

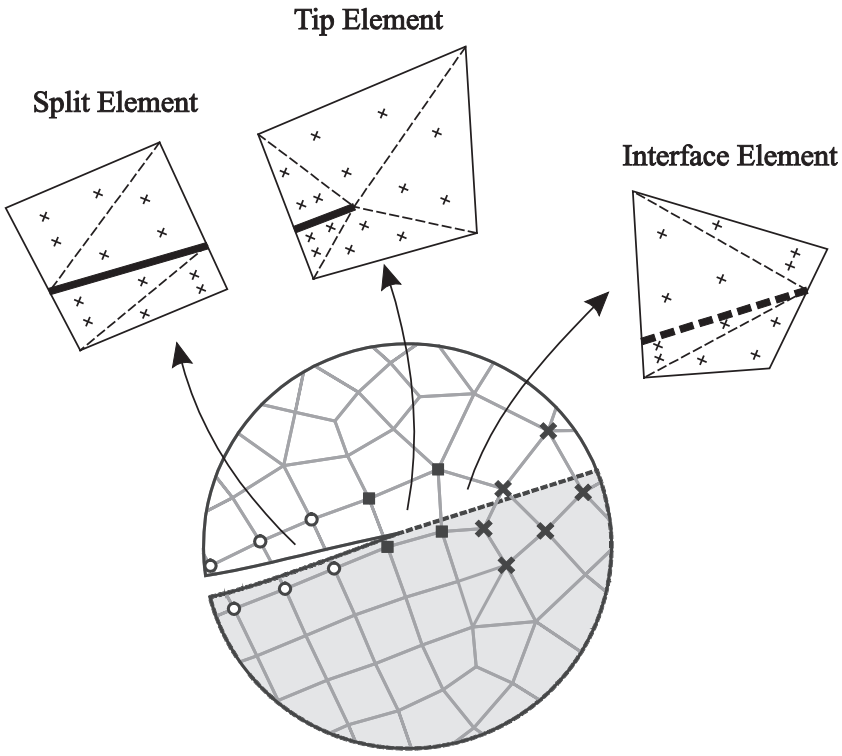

Fig. 4. Partitioning of enriched elements for numerical integration.

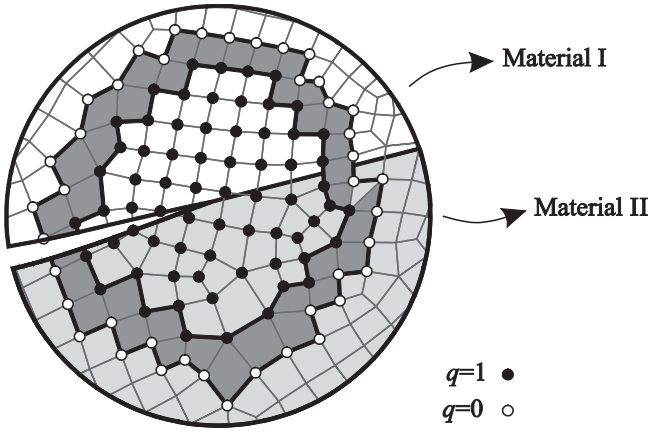

Fig. 5. Typical form of q function for numerical evaluation of the interaction integral.

$$I = \frac{H_{22}}{2\cosh^2(\pi\varepsilon)}\left(K_1 K_1^{\text{aux}} + K_2 K_2^{\text{aux}}\right) \tag{38}$$

through the use of two auxiliary fields

$$\begin{cases} I = \frac{H_{22}}{2\cosh^2(\pi\varepsilon)} K_1 (K_1^{\text{aux}} = 1;\ K_2^{\text{aux}} = 0) \\ I = \frac{H_{22}}{2\cosh^2(\pi\varepsilon)} K_2 (K_1^{\text{aux}} = 0;\ K_2^{\text{aux}} = 1) \end{cases} \tag{39}$$

7. Numerical simulations

7.1. Interface cracks with vanishing oscillatory index

This section is devoted to analysis of stationary interface cracks with a zero oscillatory index. All layers of the multi-layered material are considered to have the same orthotropic material properties, but with a 90° rotation for material axes (with respect to global coordinates in Fig. 1).

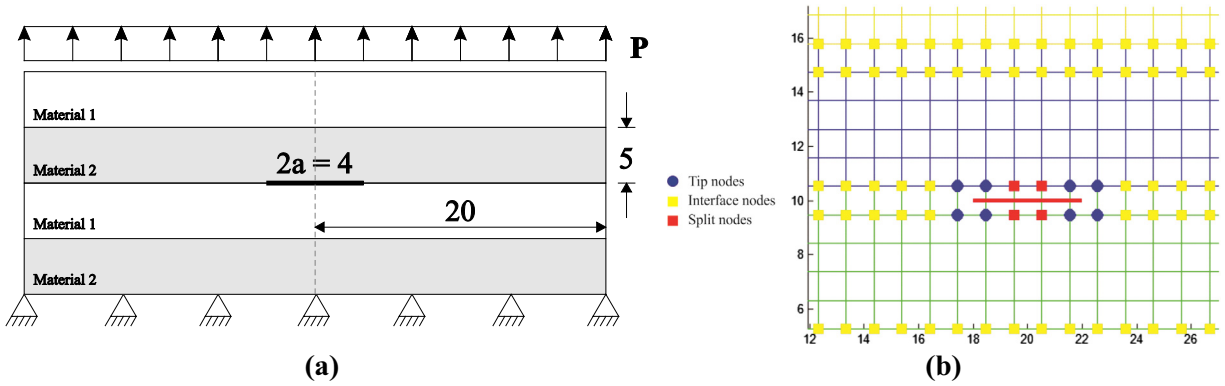

Fig. 6. (a) Geometry and boundary condition of the specimen (all dimensions in mm); (b) XFEM mesh around the crack to reproduce singularity, strong and weak discontinuity enrichments.

7.1.1. A center interface crack in a four-layer composite

In this example, the problem of an interface crack in an orthotropic solid with four layers is analyzed. Geometry and boundary conditions (Fig. 6a) are similar to Ref. [37]. The material has the following elasticity matrix in its principal material axis

$$\mathbf{C} = \begin{bmatrix} 155.43 & 3.72 & 0 \\ & 16.34 & 0 \\ \text{sym} & & 7.48 \end{bmatrix} \text{(GPa)} \tag{40}$$

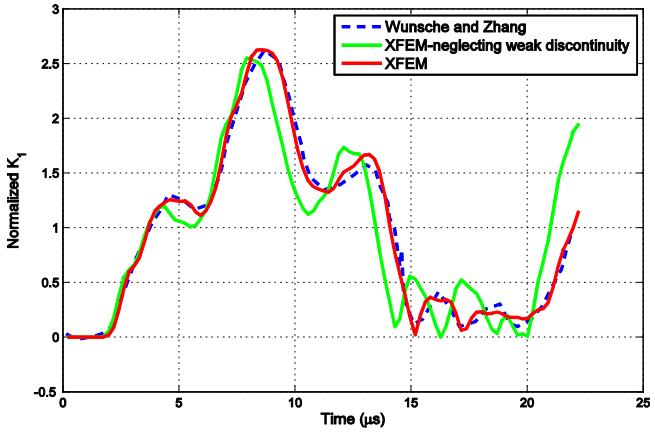

Fig. 7. Error introduced into the results by disregarding the weak-discontinuity enrichments.

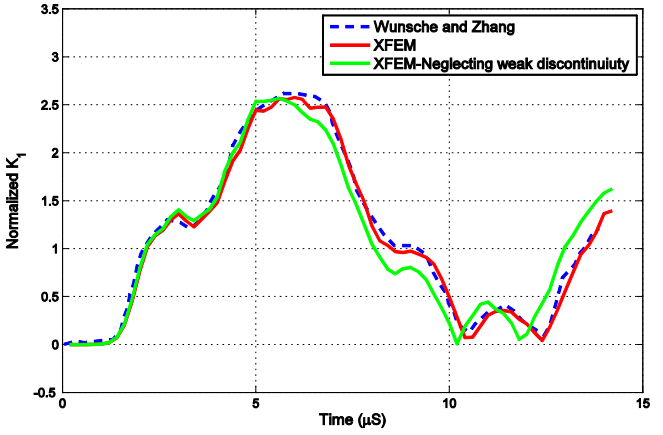

Fig. 10. Error introduced into the results without the weak-discontinuity enrichments.

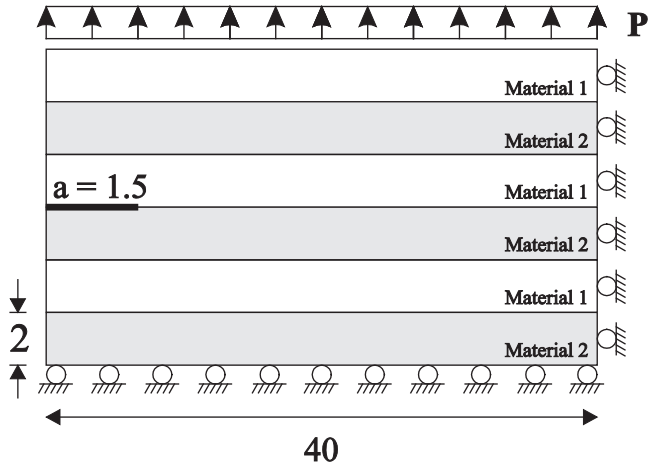

Fig. 8. Geometry and boundary condition of the six-layer specimen. All dimensions are in mm.

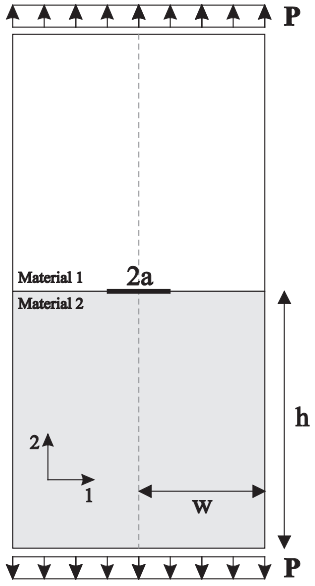

Fig. 11. Configuration of the problem.

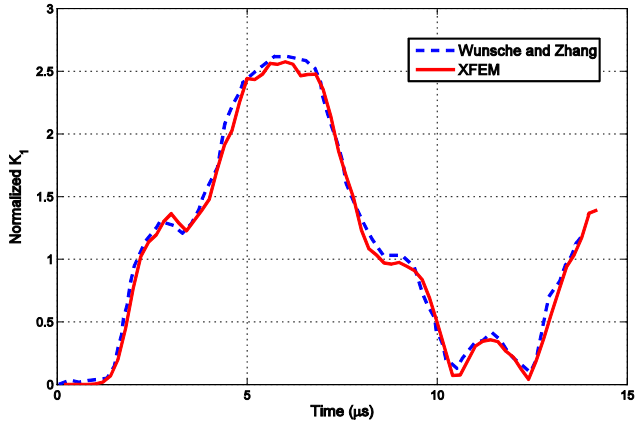

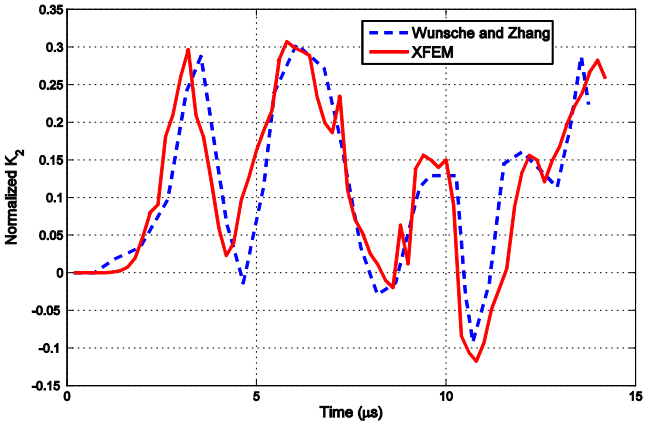

Fig. 9. Comparison of complex SIFs for the six-layer specimen.

Table 1
Geometry and the material properties for case I.

Geometry			Material 1					Material 2				
W (mm)	h (mm	a (mm)	C_{11} (GPa)	C_{12} (GPa)	C_{22} (GPa)	C_{33} (GPa)	ρ (kg/m^3)	C_{11} (GPa)	C_{12} (GPa)	C_{22} (GPa)	C_{33} (GPa)	ρ (kg/m^3)
10	20	2.4	122.77	3.88	16.34	6.94	1600	65.41	4.29	16.34	5.58	1600

Table 2
Geometry and the material properties for case II.

Geometry			Material 1					Material 2				
W (mm)	h (mm)	a (mm)	C_{11} (MPa)	C_{12} (MPa)	C_{22} (MPa)	C_{33} (MPa)	ρ (kg/m^3)	C_{11} (MPa)	C_{12} (MPa)	C_{22} (MPa)	C_{33} (MPa)	ρ (kg/m^3)
5	10	2	104.71	15.71	52.35	10	1	104.71	14.06	46.90	9.53	1

Each layer will have 0° or 90° rotation with respect to the global geometric coordinates ($\theta^{\text{material 1}} = 0°$ and $\theta^{\text{material 2}} = 90°$). The mass densities of two materials are also identical

$$\rho_1 = \rho_2 = 1600\ (\text{kg/m}^3) \tag{41}$$

The problem is solved using the uniform mesh of 40 × 20 elements (shown in Fig. 6b), 0.22 μs time-step and the J-integral domain of 2 mm. Comparison of the SIFs (normalized by $P\sqrt{\pi a}$) obtained from the J-integral and displacement extrapolation technique is depicted in Fig. 7, which shows very good agreement.

Special elements must be employed in the context of XFEM (non-conformal mesh) to provide weak discontinuity across material interfaces. Since in a dynamic analysis, a small error in the early steps of analysis accumulates and may become significant in later steps, weak discontinuity enrichment should not be disregarded in analysis of cracked layered media using XFEM. To show the significance of this enrichment, the current problem is also solved with similar conditions, except for the weak discontinuity enrichment to be neglected. Obtained normalized results, as depicted in Fig. 7, show an increasing difference with the reference values with time, proving the importance of using weak-discontinuity enrichments in a dynamic analysis with non-conformal meshes.

7.1.2. An edge interface crack in a six-layer composite

The previous example is now extended to the mixed-mode edge crack in a six-layer orthotropic solid, as depicted in Fig. 8. The material properties are the same as the previous example. This example was examined in Ref. [37] with the displacement extrapolation technique. The dynamic finite element analysis is performed by a 30 × 60 uniform mesh, 0.2 μs time step, plane strain condition and domain integral radius of 1.2 mm.

Normalized stress intensity factors (normalized by $P\sqrt{\pi a}$) are presented and compared with Ref. [37] in Fig. 9. While good agreement is observed for the real part of the SIF, the imaginary part of the obtained SIF slightly differs from the reported results. This deviation may be attributed to the inherent inaccuracy of the displacement extrapolation technique in obtaining the SIF directly from the crack tip fields.

In order to further study the effects of interface enrichments in XFEM, the same problem is solved without using the weak discontinuity enrichment and the results are presented in Fig. 10. This Figure again shows how the use of weak discontinuity enrichment in a non-conformal mesh improves the results.

7.2. Interface cracks with non-vanishing oscillatory index

A large number of bi-materials used in the industry have a non-zero oscillatory index. Therefore, the rest of examples are devoted to the analysis of bi-materials with non-vanishing oscillatory index. Additionally, in order to further demonstrate the robustness of the approach for bi-materials with relatively large values of oscillatory indices, two mixed mode configurations, subjected to impact loading, are also studied.

7.2.1. A center interface crack in an orthotropic bi-material

First, a center interface crack in an orthotropic bi-material is considered, as shown in Fig. 11. Upper and lower layers are loaded with a tensile traction. This example has been analyzed in the literature with two different geometry and material properties, using the time-domain boundary element and the displacement extrapolation technique. Geometry and material properties for two cases

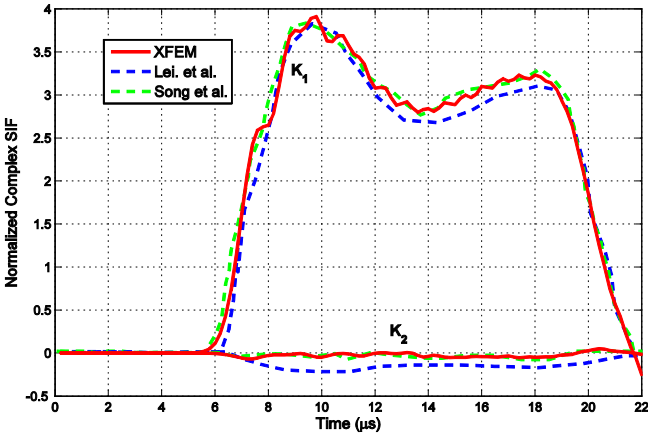

Fig. 12. Comparison of SIFs for the bi-material configuration.

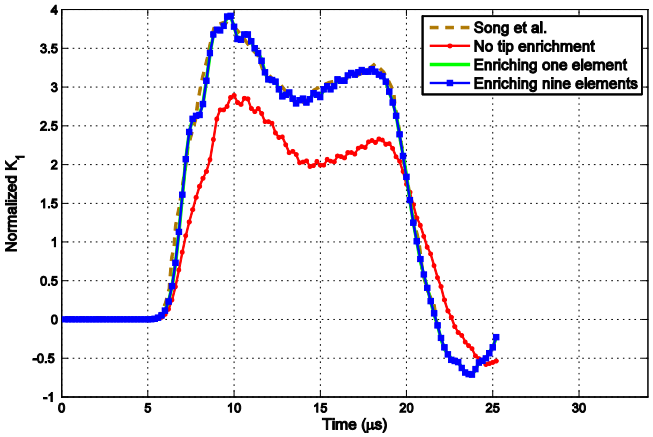

Fig. 13. Effect of different enrichment strategies.

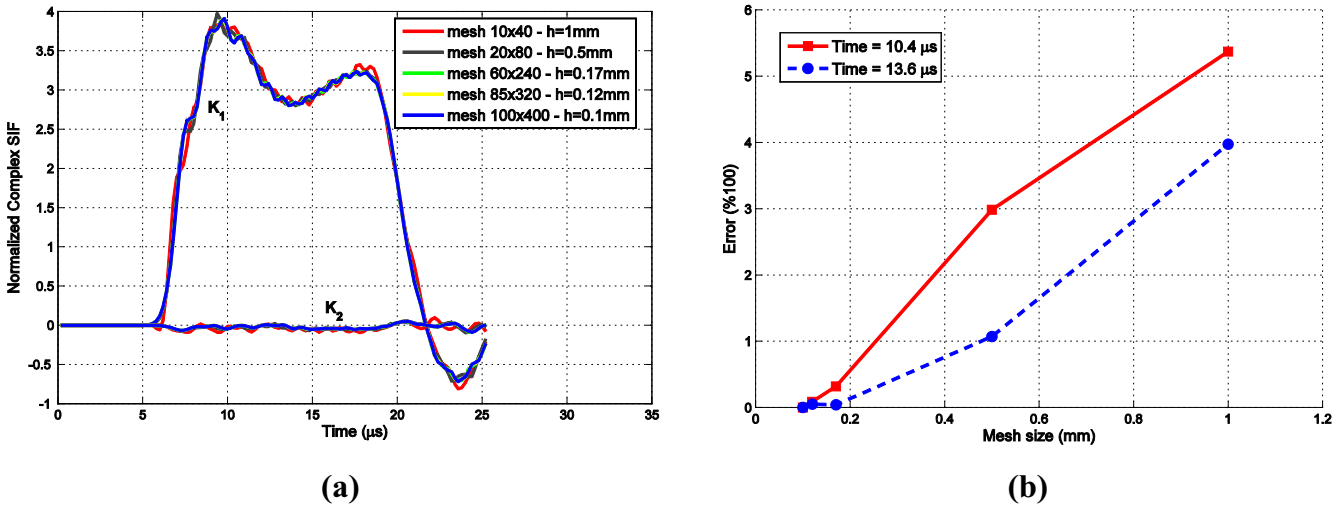

Fig. 14. (a) The predicted complex SIF for five mesh sizes; (b) error of K_1 ($Error = (K_1 - K_{1(\text{finest mesh})})/K_{1(\text{finest mesh})}$) versus the mesh sizes.

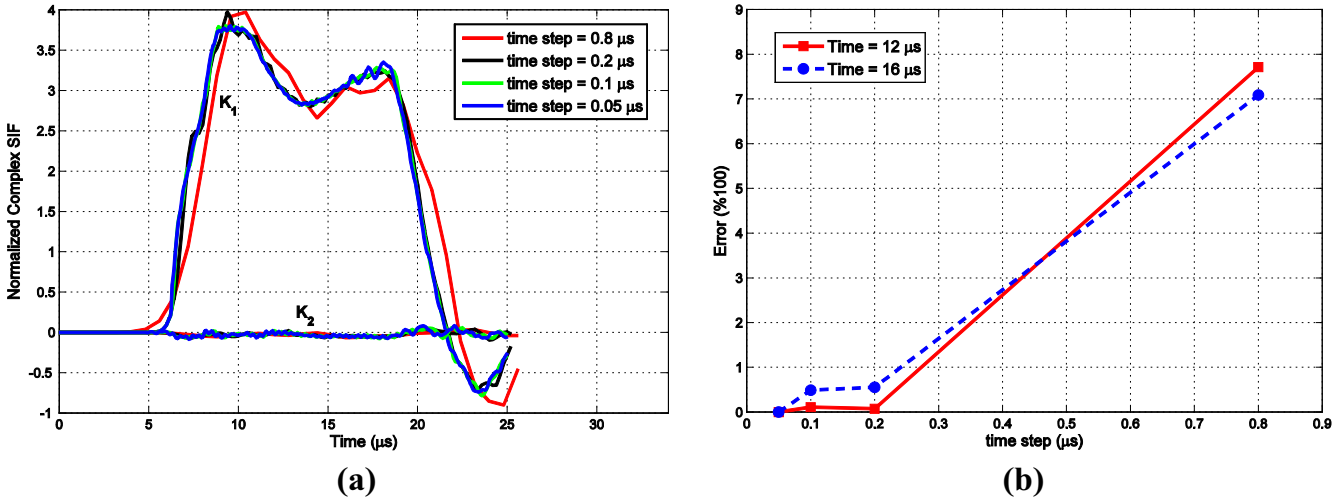

Fig. 15. (a) The predicted complex SIF for four time steps; (b) error of K_1 ($Error = (K_1 - K_{1(\text{smallest time step})})/K_{1(\text{smallest time step})}$) versus the time steps.

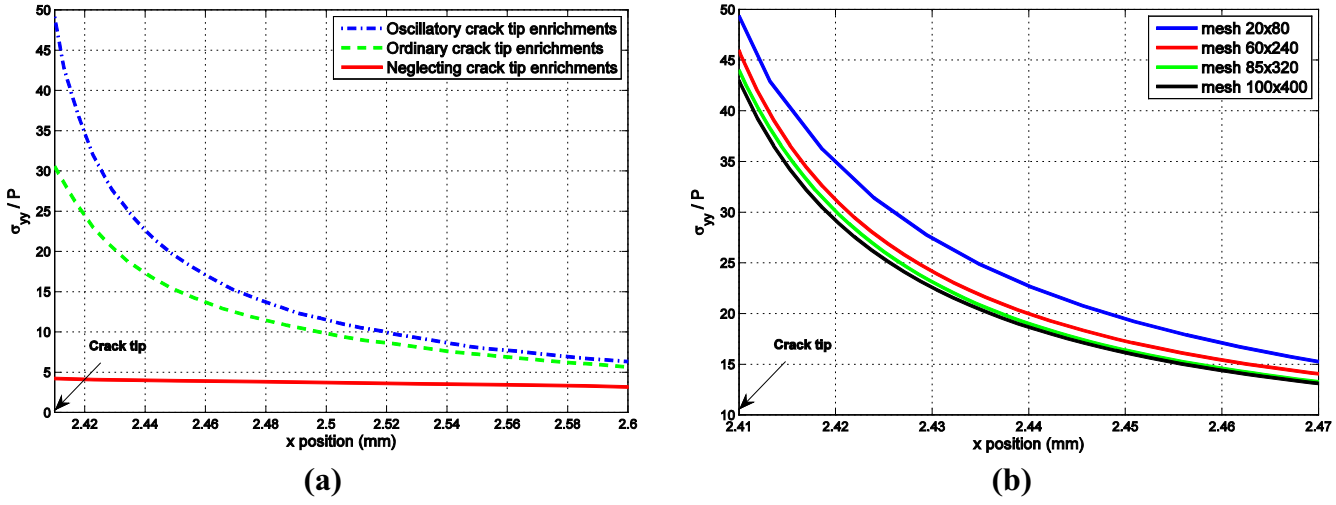

Fig. 16. (a) Effect of different crack tip enrichments on reproducing stress singularity; (b) stress distribution near the crack tip for four different meshes in case of oscillatory crack tip enrichments.

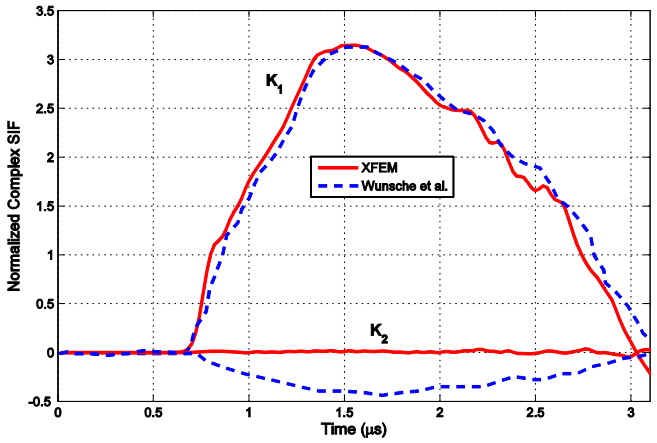

Fig. 17. Comparison of SIFs for the bi-material configuration.

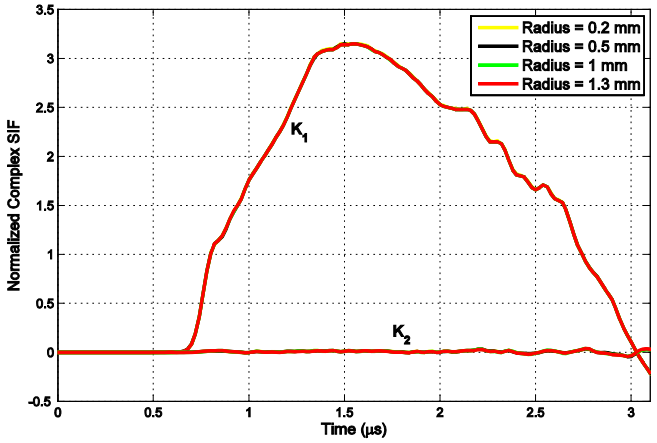

Fig. 18. The predicted complex SIF for four J-integration radii.

are presented in Tables 1 and 2. In this example, all the results related to the SIF are normalized by $P\sqrt{\pi a}$.

The corresponding oscillatory indices for two cases are $\varepsilon = 0.0137$ and $\varepsilon = 0.002$, respectively. The first case was analyzed by [10,11] with the time-domain boundary and the scaled boundary-finite element method. Although both works [10,11] used the displacement extrapolation technique to obtain complex stress intensity factors, Ref. [10] failed to incorporate the oscillatory field into the formulation. Ref. [11], however, managed to do so by expressing the oscillatory behavior of the stress field in the radial direction analytically. The difference between these two approaches is examined here by solving the same problem with XFEM, which incorporates the asymptotic functions of the crack tip in its approximation.

Half of the geometry is modeled by 60×240 elements, 0.2 μs time step, plane stress condition, and using a domain integral of 1 mm. The predicted complex SIF, which is extracted from the interaction integral, is compared with the reference results in Fig. 12. It is evident that the results of reference [11] agree well with the results obtained in the present study. It shows that in bi-materials with non-vanishing oscillatory index (even with small values of ε, as in the present case), neglecting the oscillatory nature of the field variables could result in inaccurate results (such as [10]), especially for the displacement extrapolation technique in which SIF is determined from values near the crack tip. Moreover, since this specimen is loaded in pure tension and the principal orthotropic axes are parallel to the crack, a pure mode-I fracture is expected. Although the real and imaginary parts of the complex SIF do not have the notion of mode-I and mode-II fracture in interface cracks, due to the small value of ε, it would be reasonable to expect a very small value for k_2. However, results obtained by Ref. [10] introduced non-zero spurious small k_2, mainly caused by the inherent inaccuracy of the displacement extrapolation technique and neglecting the oscillatory nature of near crack tip fields.

To further demonstrate the effects of tip enrichments, the problem is solved in three different cases: no tip enrichment function,

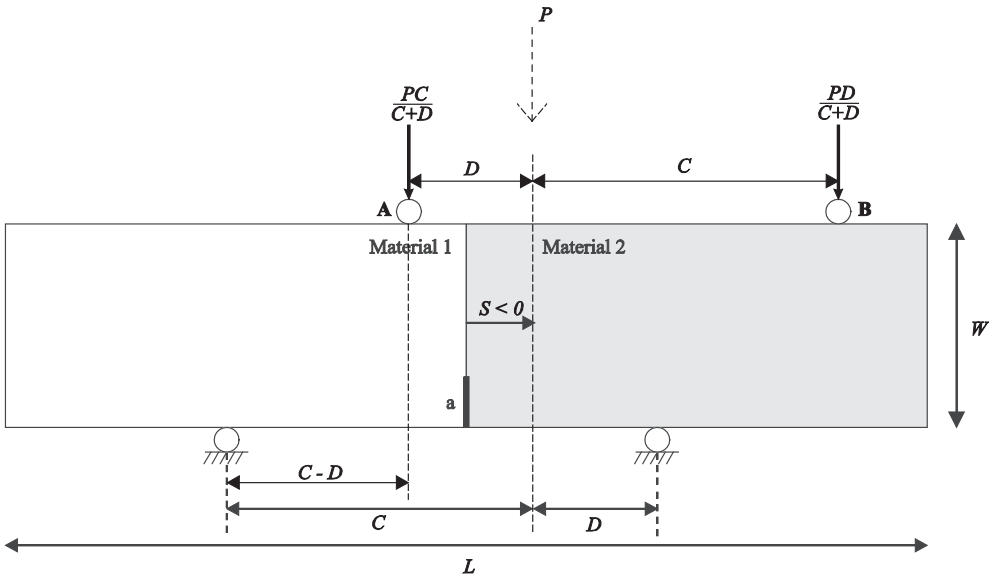

Fig. 19. Geometry and boundary condition of the specimen. (negative S/W).

Table 3
Geometry and the material properties.

Geometry				Material 1		Material 2	
W (mm)	C (mm)	D (mm)	L (mm)	E^1 (GPa)	υ^1	E^2 (GPa)	υ^2
100	1.27W	0.63W	600	3.33	0.35	80	0.3

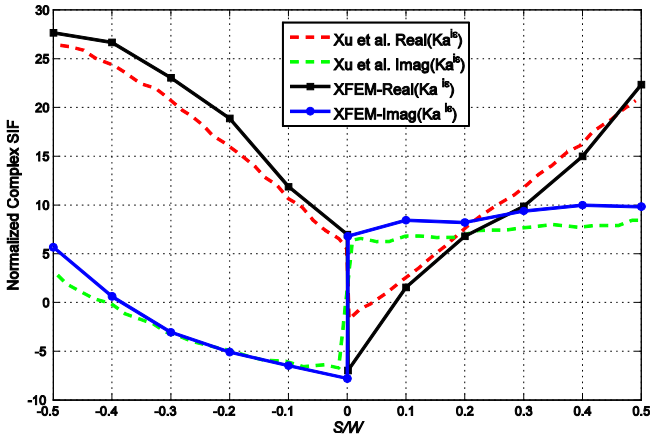

Fig. 20. Comparison of SIF values for verification of the static case.

enriching element containing the crack tip, and enriching all elements near the crack tip (9 elements). A small J-domain of 5 mm is chosen for all three cases and the results are presented in Fig. 13. It should be noted that choosing a larger domain of J-integral, mitigates the sensitivity of the results to the choice of enrichment strategy; however, it also increases computational effort dramatically. As illustrated in Fig. 13, while enriching more than one element does not alter the results, neglecting the crack tip enrichment functions substantially decreases the accuracy. Therefore, if one wants to choose a small domain of J-integral to save the computational effort throughout a dynamic analysis, enriching only the tip element seems the best strategy.

To demonstrate the mesh independency, this problem is further extended using different meshes (10×40, 20×80, 60×240 as the reference mesh, 85×320 and 100×400 elements). Fig. 14a shows the predicted complex SIF for different meshes. It is observed that the solution is not sensitive to the FE mesh sizes. Also, to examine the convergence of the solution in space, the error of K_1

Table 4
Material properties and impact loading.

PSM-1			Scotch ply 1002					Impact loading
E (GPa)	G (GPa)	ρ (kg/m^3)	E_{11} (GPa)	E_{22} (GPa)	G_{12} (GPa)	υ_{12}	ρ (kg/m^3)	P (KN/m)
2.5	0.91	1200	39.3	9.7	3.1	0.25	1860	1

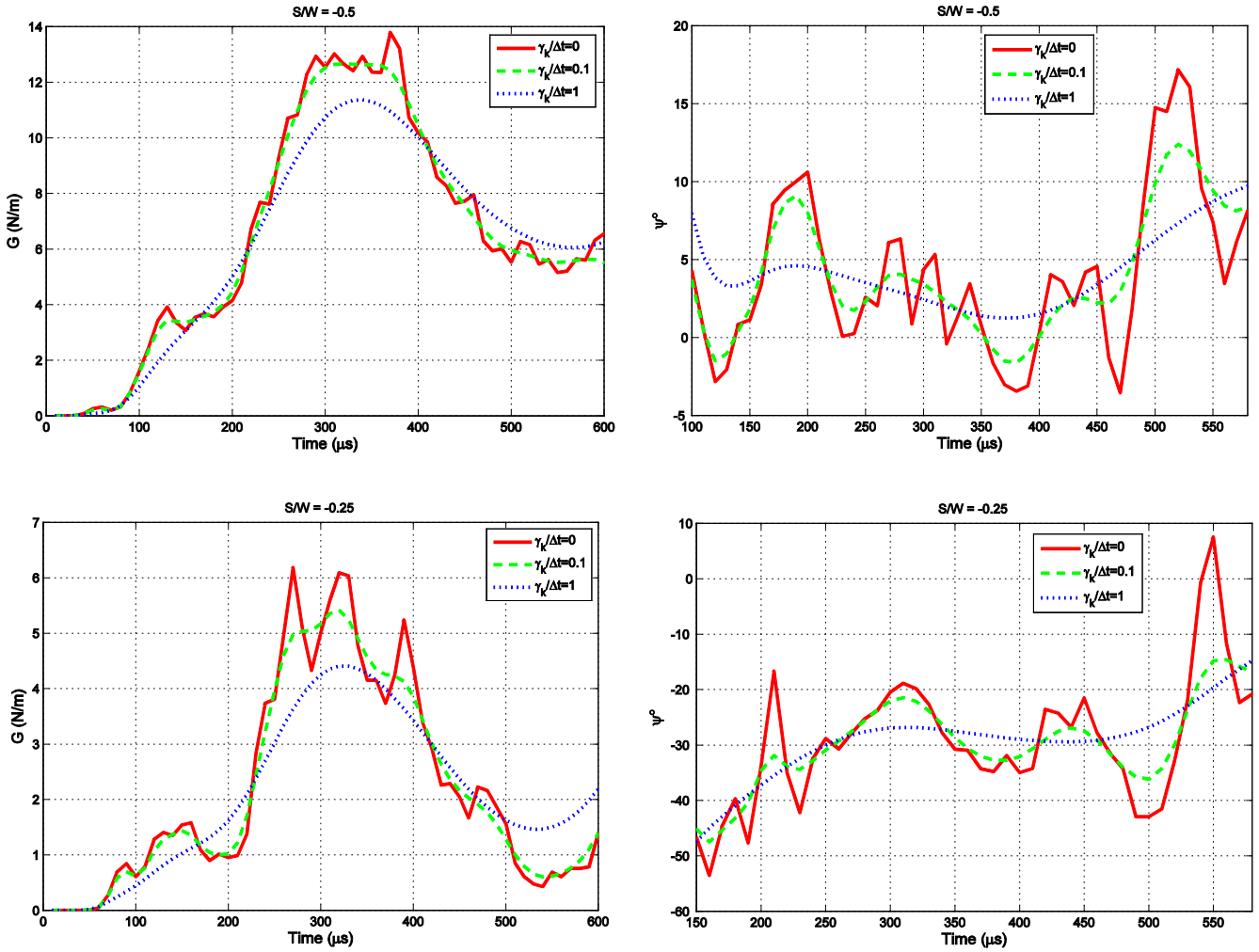

Fig. 21. Time histories of energy release rate and phase angle.

($Error = (K_1 - K_{1(\text{finest mesh})})/K_{1(\text{finest mesh})}$) versus different mesh sizes for times 10.4 μs and 13.6 μs is shown in Fig. 14b. It is expectedly observed that K_1 converges to the finest mesh as the mesh becomes finer.

To investigate the convergence of the solution in time, the predicted complex SIF is shown in Fig. 15a for four time steps (0.8 μs, 0.2 μs, 0.1 μs and 0.05 μs). It is observed that the result related to the largest time step is very different from other results and the results almost coincide as the time step is reduced. Fig. 15b illustrates the error of K_1 ($Error = (K_1 - K_{1(\text{smallest time step})})/K_{1(\text{smallest time step})}$) versus the time steps for times 12 μs and 16 μs. It can be seen that K_1 converges to the solution for the smallest time step as the time step decreases.

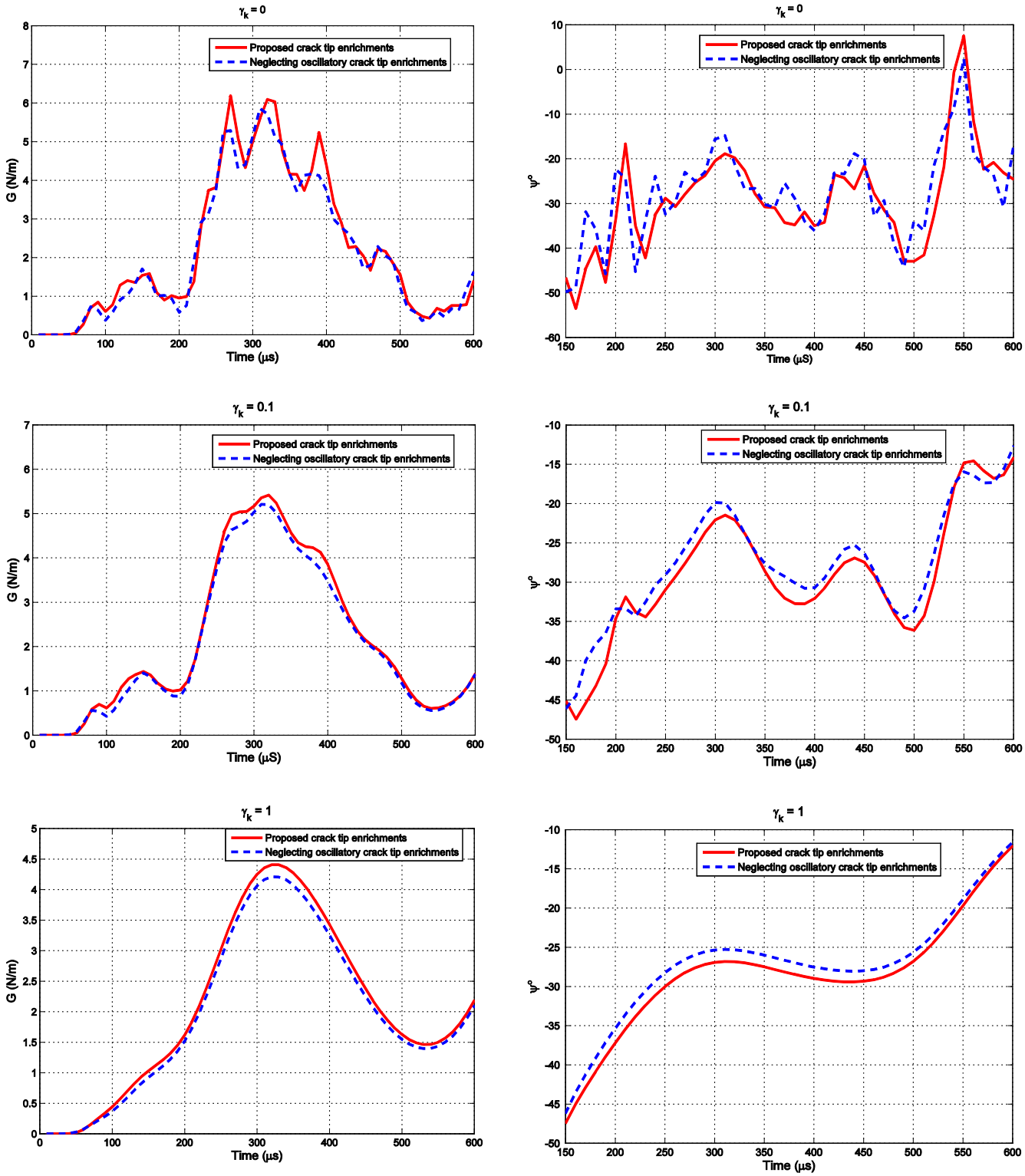

Fig. 22. Effects of oscillatory tip enrichments for different values of damping.

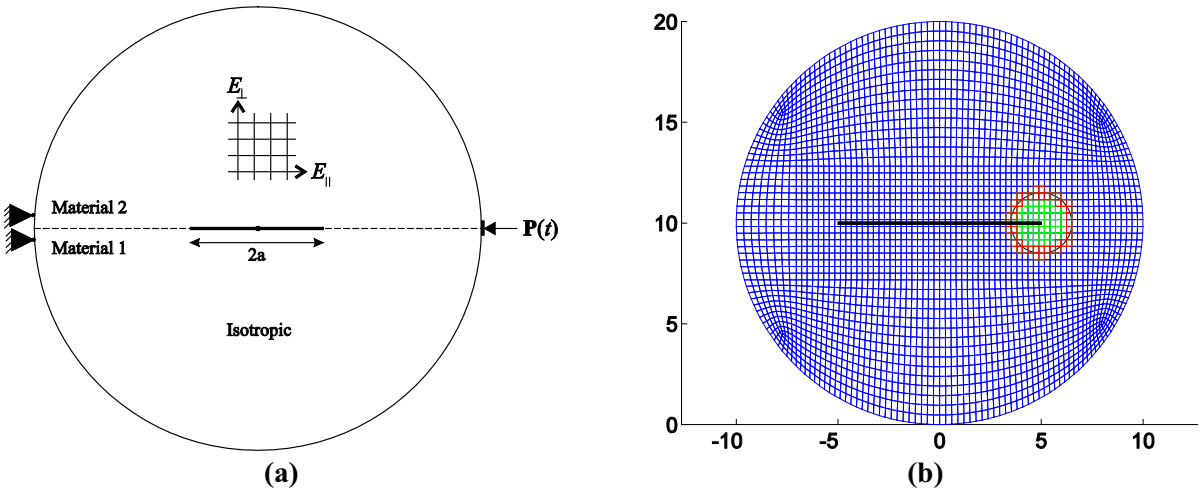

Fig. 23. (a) Geometry and boundary condition; (b) mesh and the J-integral domain.

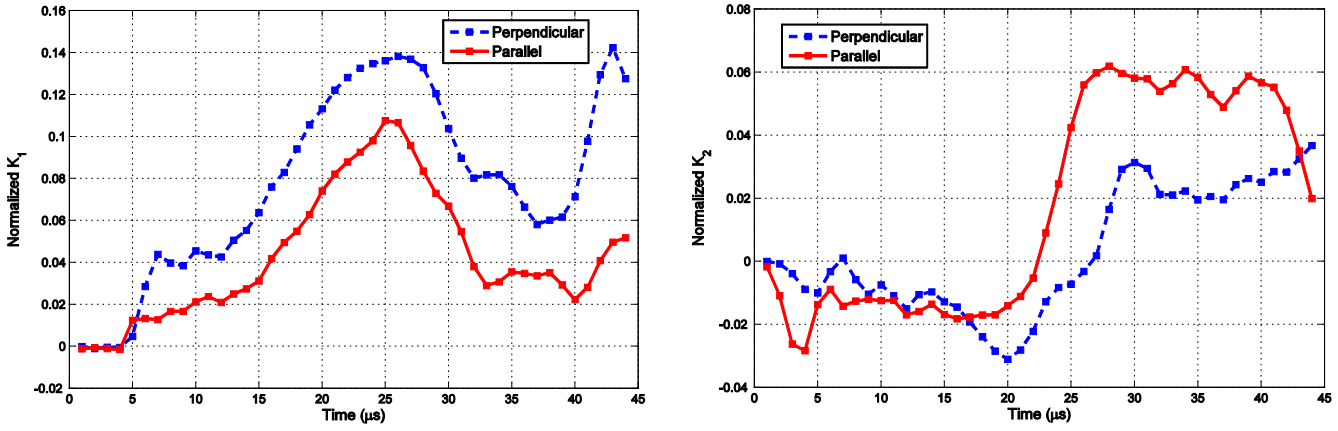

Fig. 24. Effects of fibers direction on stress intensity factors.

Table 5
Geometry and the material properties.

Geometry	Material 1		Material 2		
R (mm)	E (GPa)	ν	$E_{\parallel}$ (GPa)	$E_{\perp}$ (GPa)	ν
10	2.76	0.38	7	30	0.25

To further demonstrate the effects of the employed oscillatory crack tip enrichments, the σ_{yy} stress near the crack tip in the upper material (normalized by P), at time 15 μs, is depicted in Fig. 16a for three cases: neglecting all crack tip enrichments, neglecting only oscillatory crack enrichments and using standard orthotropic crack tip enrichments, and using full oscillatory crack tip enrichments. It is obvious that neglecting crack tip enrichments removes the crack tip singularity. Using ordinary orthotropic crack tip enrichments, however, reproduces singularity but underestimates the stress values. Finally, it is the oscillatory crack tip enrichment that reproduces the right order of singularity. In Fig. 16b, the stress distribution σ_{yy} (normalized by P) near the crack tip (at the distance of 0.06 mm from the crack tip associated with the crack tip element for mesh 100×400) at time 15 μs is shown for four different meshes. This figure is for the case of full oscillatory crack tip enrichments. As a result, the stress distribution converges to the values associated with the finest case.

The second case was studied in Ref. [38] using the boundary element method, the displacement extrapolation technique for extracting SIFs and the time step of 0.02 μs. In this study, a 30×60 mesh, along with a 0.04 μs time step and 0.2 mm size of the interaction integral are used to analyze the problem in plane stress condition. The obtained results are compared with the reference values [38] in Fig. 17. Ref. [38] used the standard boundary element method (neglecting the oscillatory behavior), which in combination with the sensitive displacement extrapolation method resulted in a non-zero imaginary part for SIF. It should be noted that the oscillatory index of the present case ($\varepsilon = 0.002$) is smaller than the previous one, so given the problem configuration, an almost zero imaginary part of the complex SIF is expected.

To demonstrate the path independency, this case is simulated using different J-integration radii (0.2 mm, 0.5 mm, 1 mm and 1.3 mm), and the results are shown in Fig. 18. It is observed that

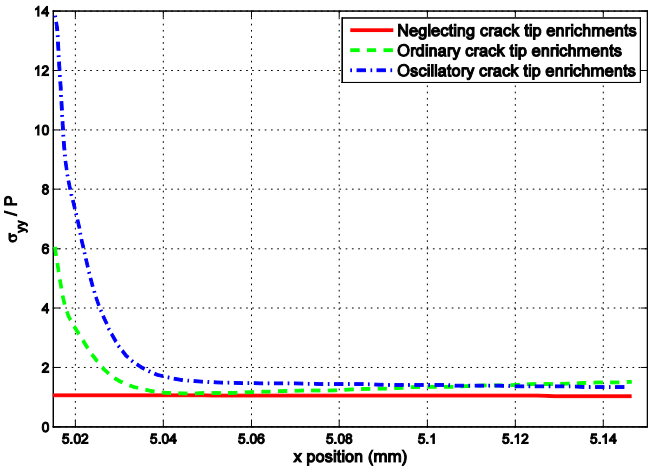

Fig. 25. Effect of different crack tip enrichments on reproducing stress singularity.

the solution is not sensitive to the integration radius and there is no path dependency.

7.2.2. Asymmetric four-point-bending specimen

The examples have so far been limited to layered plates with simple configurations. The remaining simulations are then devoted to mixed-mode test problems with more complex geometry and configurations. First, an asymmetric four-point bending specimen under the dynamic loading is considered to analyze the effects of geometry on energy release rate and phase angle history.

To verify the numerical calculation, first an isotropic bi-material beam (Fig. 19) with a static loading is solved. In Fig. 19, parameter S is changing and parameters C and D are constant. While, the overall distance between the two loads and two supports, i.e. C + D, remains constant, the beam moves with respect to the loading setup. The relative movement of the beam with respect to the loading setup is determined by S. If parameter S is on the right side of the crack, it assumes a negative value, and if it is on the left side of

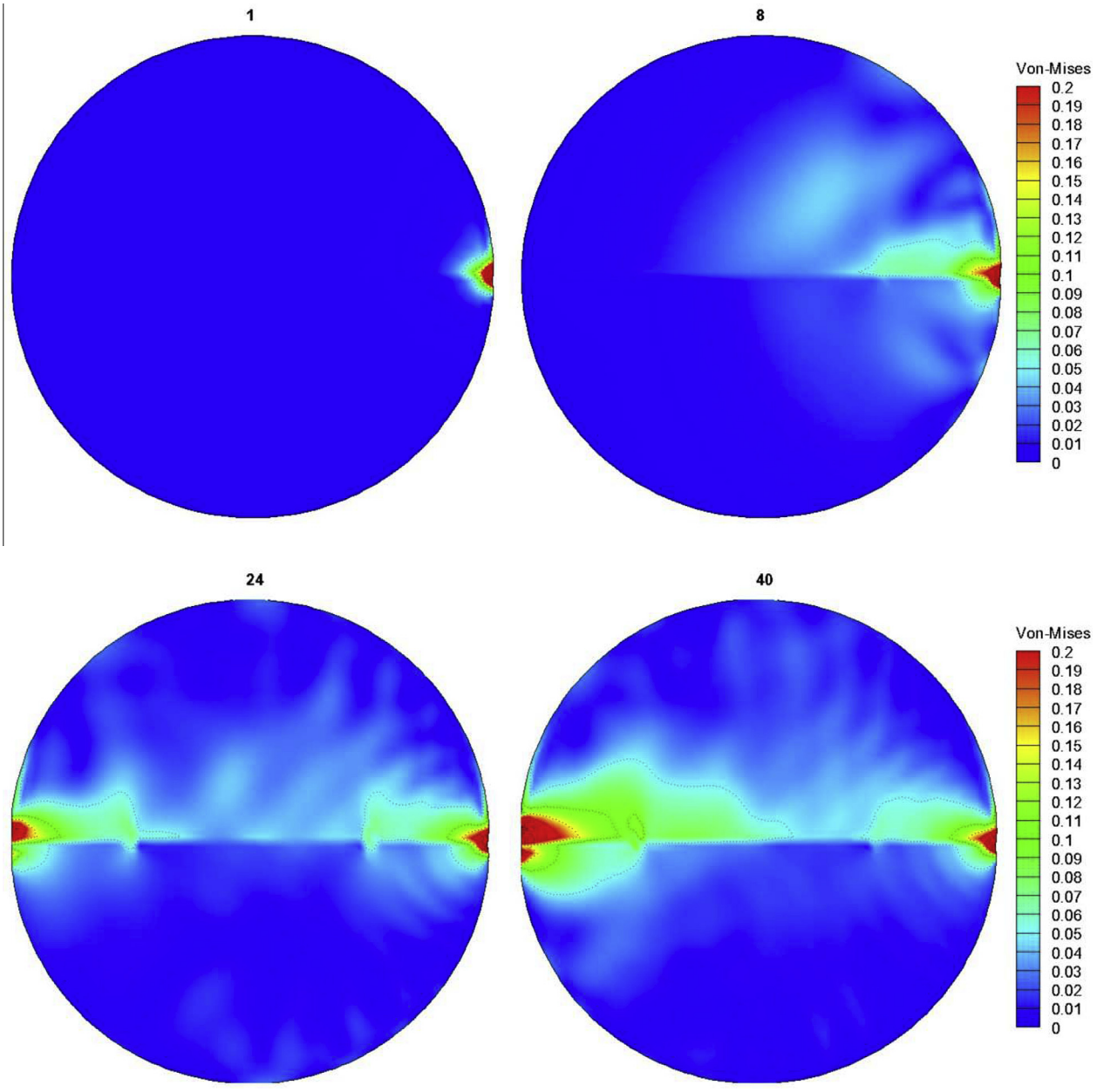

Fig. 26. Contours of von-Mises stress in different time steps (time steps in μs and stress in GPa).

the crack, it assumes a positive value. Corresponding geometric and materials properties are presented in Table 3.

Analysis is performed in the plane stress condition with 6 mm out of plane thickness. The characteristic length is assumed to be the crack length. Variations of the stress intensity factors (normalized by $P\sqrt{a}/W^2$) are presented in Fig. 20. Clearly, a good agreement exists between the present and reference [39] results.

Next, the example is extended to the impact loading $PH(t)$. Moreover, since the proposed enrichment functions are capable of producing stress and displacement fields in orthotropic bi-materials, a PSM-Scotchply bi-material (layers 1 and 2, respectively) is considered for this problem. Geometric properties are similar to those of the static case, but the material properties, which results in a large value of $\varepsilon = 0.07$, and impact loading are listed in Table 4.

The dynamic analysis is performed on a 100×20 mesh, with 10 μs time step in plane stress condition and a domain integral radius of 5 mm. Results for two cases of $S/W = -0.5$ and $S/W = -0.25$ are provided in Fig. 21, in which time histories of both the energy release rate and the phase angle are presented.

All results are compared with each other for different values of damping ($\gamma_k \neq 0$ and $\gamma_m = 0$). As expected, introducing damping into the dynamic equilibrium equation diminishes large oscillations.

As the oscillatory index of this example has quite a large value, the effects of oscillatory crack tip enrichments are discussed for the case of $S/W = -0.25$. Results of neglecting the crack tip oscillatory behavior are presented in Fig. 22 for different values of damping. It is observed that in structures with larger damping coefficients, the effect of neglecting crack tip oscillatory behavior becomes insignificant.

7.2.3. Brazilian specimen

For the last example, the bi-material Brazilian specimen, developed for analyzing mixed-mode interface cracks, is simulated. Fig. 23 depicts the geometry, boundary condition and the utilized mesh. An isotropic–orthotropic bi-material, with oscillatory index $\varepsilon = 0.057$, is considered for this problem (see Table 5).

Where $E_{\parallel}$ and $E_{\perp}$ represent the Young's modulus along and perpendicular to the fiber direction, respectively. Two cases of fibers parallel and perpendicular to the interface crack are considered. The obtained values of stress intensity factors (normalized by $P\sqrt{\pi a}$) for both cases are depicted in Fig. 24.

Clearly, when the fibers direction is parallel to the interface crack, mode-II stress intensity factor is larger. The reason can be attributed to the fact that the configuration of Brazilian test is loaded in a direction parallel to the interface crack; therefore, when the fibers are parallel to the crack the stiffness mismatch between two materials is more pronounced, resulting in shearing displacement of the crack faces and increasing the mode-II stress intensity factor.

For the case of fibers perpendicular to the interface crack, variation of the stress σ_{yy} at the time 15 μs, in the vicinity of the crack tip and in the upper material (normalized by P), is presented in Fig. 25 using three different enrichment strategies. As before, in the case of no crack tip enrichments, the stress approximation does not generate the stress singularity at the crack tip. Moreover, ordinary crack tip enrichments reproduce a stress singularity, but with an underestimation. Only in the case of oscillatory crack tip enrichments, the stress distribution is accurately reproduced.

Finally to visualize the mechanical wave propagation in the inhomogeneous material, contours of the von-Mises stress (effective stress) for time steps corresponding to $(1, 8, 24, 40)$ μs are plotted in Fig. 26.

8. Conclusion

Adopting the oscillatory crack tip enrichment functions, derived from the analytical solution of an interface crack between two orthotropic layers, and the path independent interaction integral, time histories of complex stress intensity factors, energy release rate, and phase angle have been calculated for several cracked bi-material problems subjected to dynamic loadings. It has been shown that the use of oscillatory crack tip enrichment functions, particularly in configurations with non-vanishing oscillatory indexes, can accurately reproduce the complex stress field in the vicinity of the crack tip, making the evaluation of interface fracture parameters more accurate. Moreover, numerical simulations ascertained that the interaction integral method, which utilizes the analytical solution of delamination in orthotropic bi-materials as the auxiliary field, is path-independent, and hence can be reliably adopted in mixed-mode problems, especially in comparison with the conventional displacement extrapolation technique.

Acknowledgment

The authors wish to gratefully acknowledge the technical support of the High Performance Computing Lab, School of Civil Engineering, University of Tehran. The financial support of Iran National Science Foundation (INSF) is gratefully acknowledged.

References

[1] Yuuki R, Cho SB. Efficient boundary element analysis of stress intensity factors for interface cracks in dissimilar materials. Eng Fract Mech 1989;34:179–88.
[2] Cho SB, Lee KR, Choy YS, Yuuki R. Determination of stress intensity factors and boundary element analysis for interface cracks in dissimilar anisotropic materials. Eng Fract Mech 1992;43:603–14.
[3] Ang HE, Torrance JE, Tan CL. Boundary element analysis of orthotropic delamination specimens with interface cracks. Eng Fract Mech 1996;54:601–15.
[4] Pan E, Amadei B. Boundary element analysis of fracture mechanics in anisotropic bimaterials. Eng Anal Boundary Element 1999;23:683–91.
[5] Tan CL, Gao YL, Afagh FF. Boundary element analysis of interface cracks between dissimilar anisotropic materials. Int J Solids Struct 1992;29:3201–20.
[6] Rabczuk T, Belytschko T. Cracking particles: a simplified meshfree method for arbitrary evolving cracks. Int J Numer Methods Eng 2004;61:2316–43.
[7] Rabczuk T, Belytschko T. A three-dimensional large deformation meshfree method for arbitrary evolving cracks. Comput Methods Appl Mech Eng 2007;196:2777–99.
[8] Beyer S, Zhang Ch, Hirose S, Sladek J, Sladek V. Transient dynamic analysis of interface cracks in 2-D anisotropic elastic solids by a time-domain BEM. In: Abascal R, Aliabadi MH, editor. Advances in boundary element techniques IX. UK; 2008. p. 419–26.
[9] Wünsche M, Zhang Ch, Sladek J, Sladek V, Hirose S. Interface crack in anisotropic solids under impact loading. Key Eng Mater 2007;73:348–9.
[10] Lei J, Garcia-Sanchez F, Wünsche M, Zhang Ch, Sheng Wangd Y, Saez A. Dynamic analysis of interfacial crack problems in anisotropic bi-materials by a time-domain BEM. Eng Fract Mech 2009;76:1996–2010.
[11] Song C, Tin-Loi F, Gao W. Transient dynamic analysis of interface cracks in anisotropic bimaterials by the scaled boundary finite-element method. Int J Solids Struct 2010;47:978–89.
[12] Ooi ET, Shi M, Song Ch, Tin-Loi F, Yang ZJ. Dynamic crack propagation simulation with scaled boundary polygon elements and automatic remeshing technique. Eng Fract Mech 2013;106:1–21.
[13] Chiong I, Ooi ET, Song Ch, Tin-Loi F. Computation of dynamic stress intensity factors in cracked functionally graded materials using scaled boundary polygons. Eng Fract Mech 2014;131:210–31.
[14] Areias P, Rabczuk T, Camanho P. Finite strain fracture of 2D problems with injected anisotropic softening elements. Theor Appl Fract Mech 2014;72:50–63.
[15] Areias P, Rabczuk T, Camanho P. Initially rigid cohesive laws and fracture based on edge rotations. Comput Mech 2013;52:931–47.
[16] Belytschko T, Black T. Elastic crack growth in finite elements with minimal remeshing. Int J Numer Methods Eng 1999;45:601–20.
[17] Dolbow J. An extended finite element method with discontinuous enrichment for applied mechanics. Evanston, IL, USA: Northwestern University; 1999.
[18] Afshar A, Daneshyar A, Mohammadi S. XFEM analysis of fiber bridging in mixed-mode crack propagation in composites. Compos Struct 2015;125:314–27.
[19] Asadpoure A, Mohammadi S, Vafai A. Modeling crack in orthotropic media using a coupled finite element and partition of unity methods. Finite Elem Anal Des 2006;42:1165–75.

[20] Asadpoure A, Mohammadi S, Vafai A. Crack analysis in orthotropic media using the extended finite element method. Thin-Walled Struct 2006;44:1031–8.
[21] Asadpoure A, Mohammadi S. Developing new enrichment functions for crack simulation in orthotropic media by the extended finite element method. Int J Numer Methods Eng 2007;69:2150–72.
[22] Motamedi D, Mohammadi S. Dynamic crack propagation analysis of orthotropic media by the extended finite element method. Int J Fract 2009;161:21–39.
[23] Motamedi D, Mohammadi S. Dynamic analysis of fixed cracks in composites by the extended finite element method. Eng Fract Mech 2010;77:3373–93.
[24] Motamedi D, Mohammadi S. Fracture analysis of composites by time independent moving crack orthotropic XFEM. Int J Mech Sci 2012;54:20–37.
[25] Nasirmanesh A, Mohammadi S. XFEM buckling analysis of cracked composite plates. Compos Struct 2015;131:333–43.
[26] Afshar A, Ardakani SH, Hashemi S, Mohammadi S. Numerical analysis of crack tip fields in interface fracture of SMA/elastic bi-materials. Int J Fract 2015;195:39–52.
[27] Esna Ashari S, Mohammadi S. Delamination analysis of composites by new orthotropic bimaterial extended finite element method. Int J Numer Methods Eng 2011;86:1507–43.
[28] Esna Ashari S, Mohammad S. Fracture analysis of FRP-reinforced beams by orthotropic XFEM. J Compos Mater 2012;46:1367–89.
[29] Lekhnitskii S. Theory of an anisotropic elastic body. San Francisco: Holden-Day; 1963.
[30] Lee KH, Hawong JS, Choi SH. Dynamic stress intensity factors KI and KII and dynamic crack propagating characteristics of orthotropic materials. Eng Fract Mech 1996;53:119–40.
[31] Rice JR. Elastic fracture mechanics concepts for interfacial cracks. J Appl Mech ASME 1988;55:98–103.
[32] Nakamura T, Kushner A, Lo CY. Interlaminar dynamic crack propagation. Int J Solids Struct 1995;32:2657–75.
[33] Mohammadi S. Extended finite element method: for fracture analysis of structures. John Wiley & Sons; 2008.
[34] Mohammadi S. Xfem fracture analysis of composites. John Wiley & Sons; 2012.
[35] Newmark NM. A method of computation for structural dynamics. J Eng Mech ASCE 1959;85:67–94.
[36] Lee KH. Stress and displacement fields for propagating the crack along the interface of dissimilar orthrotropic materials under dynamic mode I and II load. J Appl Mech 2000;67:223–8.
[37] Wünsche M, Zhang Ch. Transient dynamic crack analysis in piecewise homogeneous, anisotropic and linear elastic composites by a spatial symmetric Galerkin-BEM. Eng Fract Mech 2010;77:3670–86.
[38] Wünsche M, Zhang Ch, Sladek J, Sladek V, Hirose S, Kuna M. Transient dynamic analysis of interface cracks in layered anisotropic solids under impact loading. Int J Fract 2009;157:131–47.
[39] Xu L, Tippur HV. Fracture parameters for interfacial cracks: an experimental-finite element study of crack tip fields and crack initiation toughness. International Journal of Fracture 1995;71:345–63.